Journal of Environmental Management 342 (2023) 118345

Contents lists available at ScienceDirect

Journal of Environmental Management

journal homepage: www.elsevier.com/locate/jenvman

Research article

Fiber support prevents colloid-facilitated contamination induced by dissolution-precipitation of a calcium phosphate adsorbent

Eleazer L. Vivas [a], Keon-Woo Kim [a], Yong Jae Suh [b,c,**], Kuk Cho [a,*]

[a] Department of Environmental Engineering, Pusan National University, 2 Busandaehak-ro 63beon-gil, Geumjeong-gu, Busan, 46241, Republic of Korea
[b] Resources Utilization Division, Korea Institute of Geoscience and Mineral Resources, 124 Gwahak-ro, Yuseong-gu, Daejeon, 34132, Republic of Korea
[c] Department of Resources Engineering, Korea University of Science and Technology, 217 Gajeong-ro, Yuseong-gu, Daejeon, 34113, Republic of Korea

ARTICLE INFO

Keywords:
Brushite
DCPD
Cadmium
Nucleation
PAN

ABSTRACT

During the adsorptive removal of hazardous metal contaminants, dissolution–precipitation of sparingly soluble adsorbents may result in the formation of toxic colloidal suspensions, triggering secondary pollution. Therefore, we studied the prevention of colloid-facilitated contamination in a model adsorption system of dicalcium phosphate dihydrate (DCPD, $CaHPO_4{\cdot}2H_2O$) and Cd^{2+} as an adsorbent and adsorbate. Upon adding pure DCPD powder into a 500 mg L^{-1} Cd^{2+} solution of pH ≅ 7.0, aggregates of spheroidal Cd-bearing primary particles, within 0.040–0.95 μm size range, were generated via dissolution–precipitation. The accumulated volume of these submicron particles (10.8%) was greater than that of the submicron particles from the exposure of DCPD to deionized water (4.48%). While the Cd-carrying submicron particles, which are responsible for colloidal recontamination, appeared to form via homogeneous nucleation, their formation was suppressed using polyacrylonitrile fibers (PANFs) as supporting substrates. Thus, heterogeneous nucleation on PANFs formed hexagonal columnar microparticles of a new phase, pentacadmium dihydrogen tetrakis (phosphate) tetrahydrate ($Cd_5H_2(PO_4)_4{\cdot}4H_2O$). Together with dissolution–precipitation on the native DCPD, nucleation and growth on the PANFs accelerated the depletion of the dissolved species, reducing the degree of supersaturation along the DCPD-water interface. Although the PANFs decreased the Cd adsorption capacity to 56.7% of that of DCPD, they prevented the formation of small aggregates of Cd-bearing particles. Other sparingly soluble adsorbents can be compounded with PANF to prevent the generation of toxic colloids.

1. Introduction

Species dissolved from minerals, soil, sediment, and biota in water can precipitate in natural environments. This so-called dissolution–precipitation may form diverse surface structures that incorporate harmful ions such as chromate, antimonate, cadmium, arsenate, lead, uranyl, and phosphate (Astilleros et al., 2013; Guren et al., 2020; Morales et al., 2013; Renard et al., 2018; Wang et al., 2015, 2017; Zhai et al., 2018). Furthermore, dissolution–precipitation can induce colloidal dispersions of substances such as feldspar, mica, magnetite (Mashal et al., 2004), river minerals (Plathe et al., 2013), coastal soil (Wei et al., 2022), chalk (Tang and Weisbrod, 2009), nuclear melt glass (Joseph et al., 2019), tuffaceous rock (Wolfsberg et al., 2017), and used cathode ray tube glass (Yamashita et al., 2010). Thereby, harmful ions can be immobilized on the surface of native substances or incorporated into newly formed colloidal particles. Stable colloidal dispersions are highly mobile in water; thus, harmful ions incorporated into the particulate phase can be assimilated by aquatic flora and fauna (Ryan and Elimelech, 1996). Harmful species that accumulate in this way contaminate the natural environment and threaten human health. A similar situation may occur when attempting to remove hazardous materials from water via adsorption, using a sparingly soluble adsorbent. Therefore, adsorptive treatment of polluted water can lead to inadvertent recontamination by contaminant-bearing colloids. However, studies on colloid-facilitated water contamination have not extended to its prevention.

* Corresponding author. Department of Environmental Engineering, Pusan National University, 2 Busandaehak-ro 7 63beon-gil, Geumjeong-gu, Busan, 46241, Republic of Korea.
** Corresponding author. Resources Utilization Division, Korea Institute of Geoscience and Mineral Resources, 124 Gwahak-ro, Yuseong-gu, Daejeon, 34132, Republic of Korea.
E-mail addresses: aumsuh@kigam.re.kr (Y.J. Suh), kukcho@pusan.ac.kr (K. Cho).

https://doi.org/10.1016/j.jenvman.2023.118345
Received 4 April 2023; Received in revised form 25 May 2023; Accepted 6 June 2023
Available online 11 June 2023

To study colloidal contamination attributable to dissolution–precipitation, both appropriate adsorbent and adsorbate must first be selected. Calcium phosphates (CaPs) involve dissolution–precipitation in their complex interactions with metal ions (Cao et al., 2004). Among CaPs, hydroxyapatite (HAp, $Ca_{10}(PO_4)_6(OH)_2$) and brushite (dicalcium phosphate dihydrate, DCPD, $CaHPO_4{\cdot}2H_2O$) are well known adsorbents. DCPD is more susceptible to dissolution–precipitation as it has significantly higher solubility ($K_{sp} = 10^{-6.60}$) than HAp ($K_{sp} = 10^{-117}$) (Gregory et al., 1970; McDowell et al., 1977). At DCPD-water interface, simultaneous immobilization of Cd^{2+} and AsO_4^{3-} via dissolution–precipitation was recently observed (Zhai et al., 2018). Given the extreme toxicity of Cd^{2+} in water, adsorptive Cd^{2+} removals have been extensively studied using several adsorbents, including calcium-phosphate, oxalate, silicate, and carbonate (Le et al., 2021; Medellín-Castillo et al., 2020; Wang et al., 2020; Zhai et al., 2018; Zhou et al., 2022). Thus, a pair of DCPD and Cd^{2+} is considered a good candidate for studying colloid-facilitated contamination and its prevention.

Generally, the formation of colloidal particles occurs upon supersaturation of the precursor or monomers in the solution. This homogeneous nucleation-driven formation requires overcoming a large barrier of an increase in Gibbs energy of the system (Manuel García-Ruiz, 2003). On the other hand, heterogeneous nucleation on a foreign substrate is constrained by a much lower energy barrier. Hence, we hypothesized that additional surfaces from supporting solid, such as fibers would restrict the homogeneous nucleation of a new phase incorporating toxic metal ions, thereby preventing the formation of suspended particulate matters in water and precluding colloid-facilitated recontamination. Several supporting solids, such as alginate (Googerdchian et al., 2012; Li et al., 2023), polyurethane foam (Jang et al., 2008), biochar (Zhou et al., 2022), and polyacrylonitrile (PAN) (Vivas et al., 2020), have been used for the removal of Pb^{2+}, Cd^{2+}, and Sr^{2+} without considering the aforementioned hypothesis. In this study, we used water-insoluble electrospun polyacrylonitrile fibers (PANF) because of their high hydrophilicity and mechanical stability.

In this study, we exposed DCPD-infused PANFs to aqueous Cd^{2+} solutions to examine whether the DCPD/PANF composite prevents the formation of free Cd-bearing particles. Subsequently, the potential use of the DCPD/PANF composite as a Cd^{2+} adsorbent was confirmed through batch adsorption experiments under varying initial Cd^{2+} concentrations (C_0), contact time (t), and pH, and in the presence of competing cations. The results demonstrated that the colloid-facilitated contamination during adsorptive removal of toxic metal ions such as Cd^{2+} can be prevented by introducing an appropriate foreign solid for the first time.

2. Materials and methods

The materials and methods used in this study are provided in the Supporting Information. PANFs with various DCPD loadings were labeled as: DCPD(X)/PANF, where X is the DCPD loading in wt% with respect to the PAN loading.

3. Results

3.1. Properties of as-synthesized DCPD and PAN fibers

Detailed characterization results of the DCPD powder and DCPD (100)/PANF are provided in Section S2 and Fig. S1 of the Supporting Information.

3.2. Change of particle characteristics during Cd adsorption

The change in particle size distribution and settling velocity of the DCPD powder and DCPD/PANFs after soaking for 24 h in varying Cd solutions (pH ≅ 7.0) were investigated using laser diffraction particle size analysis and kinetic light extinction measurements. Fig. 1A shows

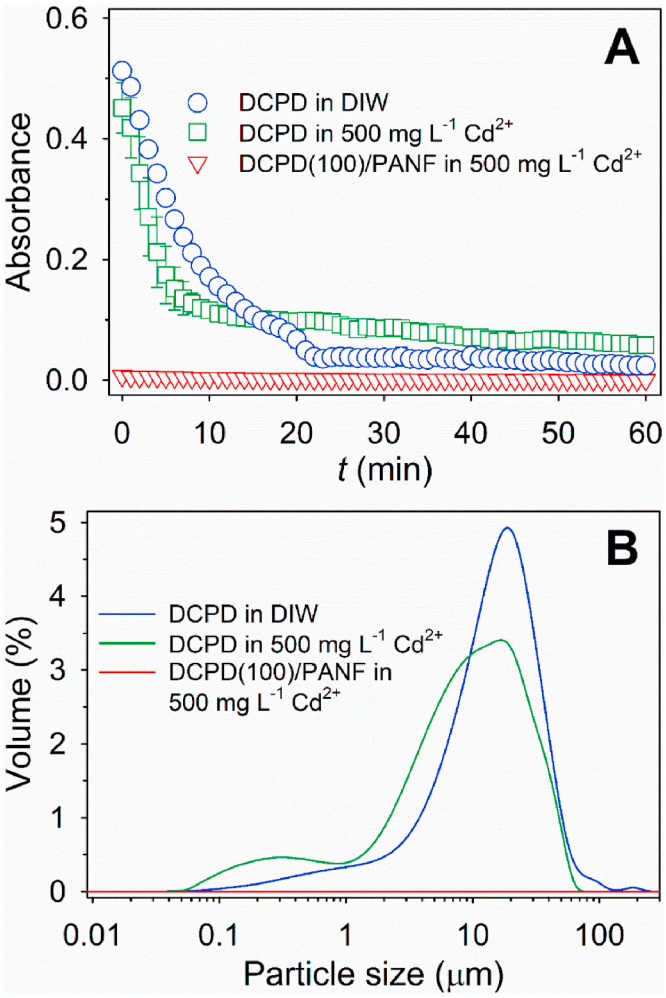

Fig. 1. Photometric characteristics of colloidal dispersions formed by the dissolution–precipitation of DCPD: (A) Kinetic light extinction profiles and (B) Size distributions of colloidal suspensions after soaking under various conditions for 24 h.

that the DCPD powders soaked in a 500 mg L^{-1} Cd^{2+} solution exhibited a steeper negative slope at the beginning of the light extinction measurement than those soaked in deionized water (DIW). On the other hand, at settling time $t \geq 15$ min, the mean absorbance for the former was 1.9 times that of the latter. This seemingly contradictory trend is attributable to the change in the PSD from a unimodal size distribution to a bimodal distribution (Fig. 1B). These DCPDs soaked in the Cd-rich solution and DIW had a mean particle size of 14.3 and 19.0 μm, respectively; while for the 0.040–0.95 μm size range, the former had greater accumulated volume (10.8%) than the latter (4.48%). The soaking in the Cd solution induced the population growth of particles smaller than ~10 μm. Of which, the source material may be supplied by dissolution of parent DCPD particles larger than 10 μm. An increase in the number of particles in the submicron range led to prolonged dispersion in water (Fig. 1A). Contrary to the general trend, the decrease in the number of particles larger than ~0.95 μm resulted in faster settling at the beginning of measurement. This opposing observation can be explained by the increased density after Cd^{2+} adsorption or the decreased repulsion between the particles because of the increased ionic strength. Meanwhile, soaking the DCPD powder in a 10 mg L^{-1} Cd^{2+} solution caused a slight change in the settling behavior (Fig. S2A), most likely because of a similar particle size distribution.

In contrast, the DCPD(100)/PANF samples soaked in a 500 mg L^{-1} Cd^{2+} solution exhibited no extinction by the suspended particles during

the kinetic extinction measurements (Fig. 1A). The PSD presented a flat curve at zero vol% because the diffraction signal was not detected, implying the absence of free suspended particles during the laser diffraction measurement (Fig. 1B). All liquid samples of DCPD/PANFs demonstrated near-zero and zero absorbance throughout the light extinction measurement period (Fig. S2B). In these analyses, DCPD/PANFs with DCPD loadings of less than 120 wt% were used because DCPD(120)/PANF was physically unstable as it underwent fiber disintegration (Fig. S5).

The changes in the morphology and composition of DCPD and DCPD/PANF during Cd adsorption were examined using a scanning electron microscope (SEM) and energy-dispersive X-ray spectroscopy (EDS) (Fig. 2). After soaking them in a 500 mg L^{-1} Cd^{2+} solution for 24 h, the morphology of most DCPD particles appeared plate-like (Fig. 2A), similar to that of the as-synthesized DCPD (Fig. S1A); a small amount of aggregates of spheroidal particles was observed (Fig. 2B), which was not observed in the pristine DCPD sample. The stacked platy particles appeared to be larger than 5.0 μm in width (Fig. 2A) while the aggregates were smaller than 0.25 μm (Fig. 2B). On the other hand, their compositions were measured at 18.6 wt% Ca and 33.3 wt% Cd in the platy microparticles (Fig. 2E) and 13.4 wt% Ca and 8.81 wt% Cd in the submicron aggregate (Fig. 2F). Both particles exhibited a significant decrease in Ca content compared to that of the as-synthesized DCPD (37.3 wt%, Fig. S1C). The larger platy particles had a much higher Cd content than the smaller aggregates, implying a greater extent of adsorption or precipitation. Although the two types of particles retained 49.9% or 36.1% of the Ca content, the XRD profiles of ample solid residues exhibited a transformation of the crystal structure (Fig. 3D and G). The adsorption of Cd resulted in crystal transformation to or precipitation of a new phase, *i.e.*, pentacadmium dihydrogen tetrakis (phosphate) tetrahydrate (PCDTP, $Cd_5H_2(PO_4)_4{\cdot}4H_2O$), which is indexed to monoclinic crystal system (ICDD: 98-001-0045) in C2/c space group (Fig. 3C and G). However, after soaking in a 10 mg L^{-1} Cd^{2+} solution for 24 h, the crystal structure of DCPD appeared to transform from brushite to monetite (dicalcium phosphate (DCP), $CaHPO_4$), which was indexed to an anorthic crystal system (ICDD: 98-003-8128) in the P-1 space group (Fig. 3B and F). Additionally, the DCPD particles soaked in DIW for 24 h appeared to have transformed into monetite (Fig. 3E). This transformation may be caused by dehydration during the drying of the powder samples after soaking, which was also observed in a 50 mg L^{-1} Co^{2+} solution in a previous study (Vivas and Cho, 2021).

When the as-prepared DCPD(100)/PANF were soaked in a 500 mg L^{-1} Cd^{2+} solution for 24 h, two types of microparticles were observed on the stacked lath-like PAN fibers: jelly-like lumps across the fibers and hexagonal columnar shapes (Fig. 2C and D). The lumpy particles were composed of 30.8 wt% Ca and 14.0 wt% Cd (Fig. 2G), indicating a lower extent of adsorption. Conversely, the hexagonal columnar particles were composed of 0.53 wt% Ca and 53.4 wt% Cd (Fig. 2H), implying a near-complete transformation or dissolution–precipitation. Given their elemental composition of $Cd_{4.9}Ca_{0.1}H_2(PO_4)_4{\cdot}4H_2O$) based on the EDS analysis, the columnar microparticles might be cadmium hydrogen phosphate hydrate or PCDTP. The XRD pattern of DCPD(100)/PANF after soaking revealed the coexistence of PCDTP and monetite (Fig. 3H and I), corresponding to a mixture of lumpy particles and columnar microparticles. Compared to DCPD, the extent of the structural transformation of DCPD(100)/PANF was slowed down. In the DCPD(100)/PANF sample, it was difficult to distinguish the submicron particles from the multi-layered network of PANFs.

3.3. Adsorption performance of DCPD(100)/PANF

Given the structural transformation of DCPD(100)/PANF in the Cd-rich solution, its adsorption performance toward Cd^{2+} was investigated using batch adsorption experiments. The Cd^{2+} uptake kinetics of DCPD(100)/PANF were examined at $C_0 = 10$ and 1000 mg L^{-1}. At $C_0 =$ 10 mg L^{-1}, the composite fibers exhibited smooth single-stage kinetics, with a Cd^{2+} removal efficiency (*RE*) of 90.9%, which was nearly saturated after 2 h (Fig. 4A). Zhai et al. (2018) also observed a rapid adsorption of Cd on the DCPD surface at low concentrations of Cd (≤50 μM). In contrast, a multistage Cd^{2+} adsorption kinetics was observed at $C_0 = 1000$ mg L^{-1}. The Cd adsorption increased initially at a sharp rate, reaching the first plateau after 1 h (*RE* = 5.54%), and after ~3 h induction period, increasing again rapidly until the second plateau was reached after 12 h with Cd^{2+} uptake escalating to *RE* = 24.6% (Fig. 4A).

Next, the maximum (q_m) and highest experimental ($q_{e,h}$) adsorption capacities of DCPD(100)/PANF for Cd^{2+} were determined via adsorption experiments at C_0 = 10–1000 mg L^{-1}. The adsorption on the composite fibers reached the highest value of $q_{e,h} = 246$ mg g^{-1} at an equilibrium concentration (C_e) of 754 mg L^{-1} (Fig. 4B). The nonlinear regressions of the equilibrium adsorption data best fitted the Sips model with the highest correlation coefficient of $r^2 = 0.992$ (Table S1). The highest experimental capacities $q_{e,h}$ were close to the maximum capacities q_m of 242 and 252 mg g^{-1} calculated using the Sips and Langmuir models, respectively (Table S1).

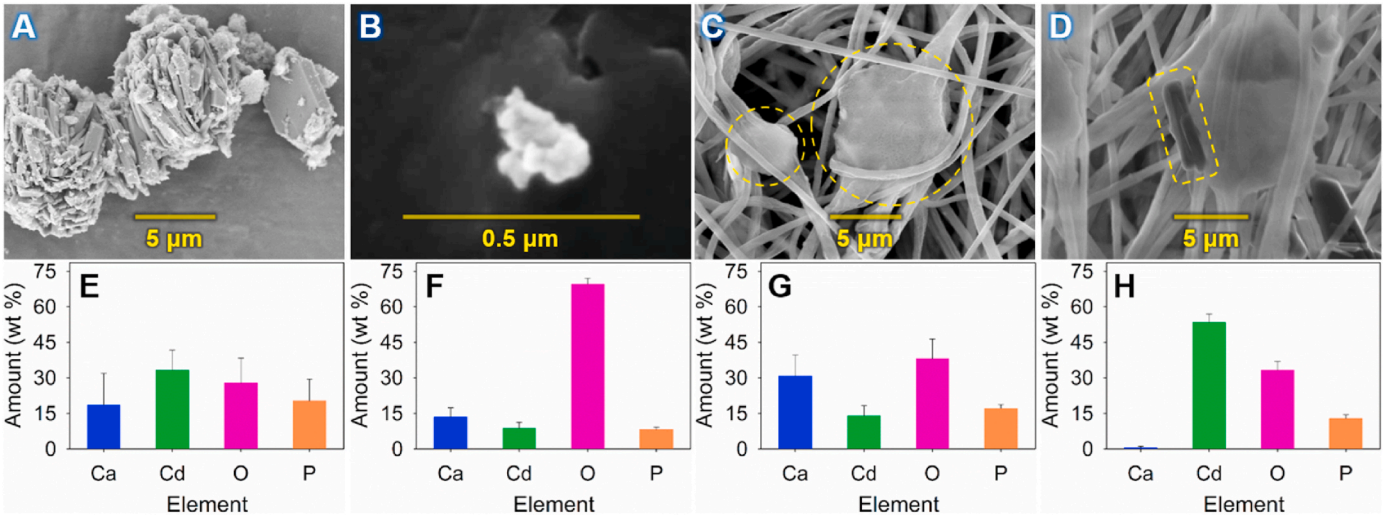

Fig. 2. SEM images and elemental compositions (EDS analyses) of Cd-bearing (A, E) microparticles and (B, F) submicron aggregate particle after adsorption using DCPD, and Cd-bearing (C, G) lumpy particles trapped by PANFs and (D, H) hexagonal columnar PCDTP particles deposited on PANFs after adsorption using DCPD (100)/PANFs. General adsorption conditions: $C_0 = 500$ mg L^{-1}, pH ≅ 7.0, $t = 24$ h, T ≅ 25.0 °C.

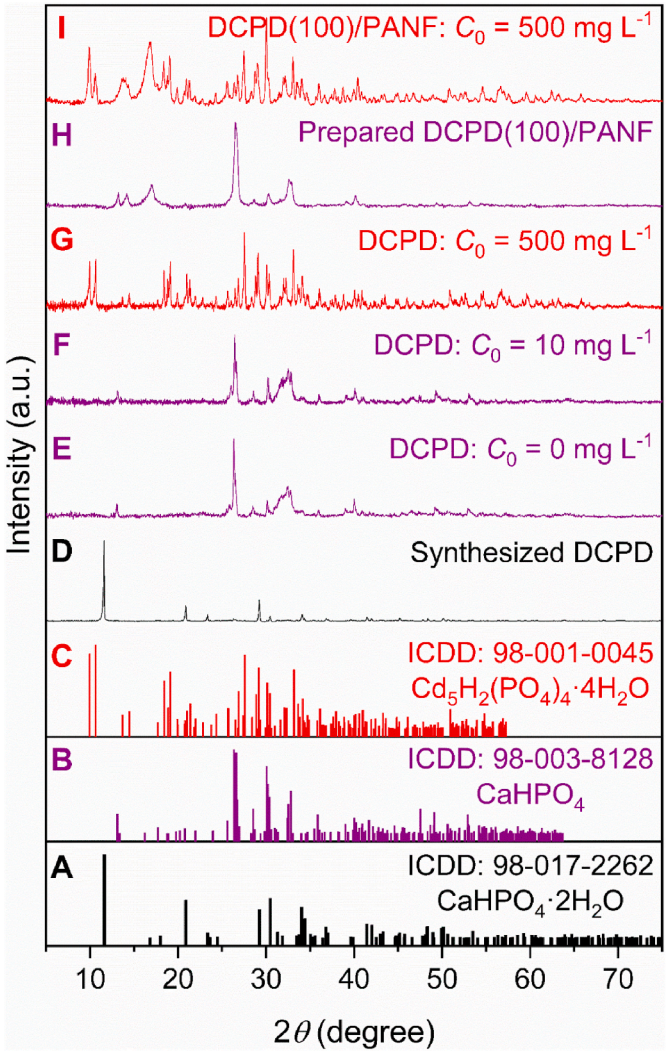

Fig. 3. Powder diffractograms: (A) Reference monoclinic brushite, (B) Reference anorthic monetite, and (C) Reference monoclinic $Cd_5H_2(PO_4)_4{\cdot}4H_2O$; (D) DCPD before soaking and (E–G) DCPD after soaking in DIW and 10.0 and 500 mg L^{-1} Cd^{2+} solutions; (H) as-prepared DCPD(100)/PANF and (I) DCPD(100)/PANF after soaking in a 500 mg L^{-1} Cd^{2+} solution. General experimental conditions: $T \cong 25.0$ °C, pH ≅ 7.0, $t = 24$ h.

The effect of pH on Cd adsorption by DCPD(100)/PANF was investigated in the pH range 3–7. In this experiment, the pH range narrowed as DCPD dissolution and Cd hydrolysis greatly interfered with the dissolution–precipitation behavior. DCPD completely dissolved in highly acidic conditions, *i.e.*, pH ≅ 2.0, and Cd^{2+} ions precipitate as cadmium hydroxide at pH > 7.0. Excluding pH 3, distribution coefficients (K_d) for Cd^{2+} at $C_0 \cong 10.0$ mg L^{-1} were nearly the same at approximately 7.32×10^4 mL g^{-1} ($RE = 98.7\%$) (Fig. 4C), indicating a strong preferential Cd^{2+} adsorption on DCPD(100)/PANF. At pH 3, K_d decreased to 2.48×10^4 mL g^{-1} ($RE = 96.1\%$), likely due to a higher dissolution of DCPD and competition for adsorption sites with protons. The H^+ concentration at pH 3 (1.0 mmol L^{-1}) was an order of magnitude higher than that of Cd^{2+} (10.0 mg L^{-1} or 0.089 mmol L^{-1}).

Finally, the interference of typical competing cations in the adsorptive Cd^{2+} removal by DCPD(100)/PANF was investigated. At a cation concentration of 10 mmol L^{-1}, the presence of Ca^{2+} and Mg^{2+} resulted in a significant decrease in K_d to 1.24×10^4 mL g^{-1} and 1.30×10^4 mL g^{-1}, respectively (Fig. 4D). In contrast, Na^+ and K^+ moderately reduced K_d to 6.09×10^4 mL g^{-1} and 6.24×10^4 mL g^{-1} (or a reduction by 16.8% and 14.8%), respectively (Fig. 4D). The inhibitory effect of divalent cations on the Cd^{2+} adsorption on the composite fiber was greater than that of monovalent cations in order of $Ca^{2+} > Mg^{2+} \gg Na^+/K^+$. As expected, the distribution coefficient decreased greatly in artificial seawater (ASW) to 301 mL g^{-1}, particularly because of the high concentrations of Ca^{2+} (8 mmol L^{-1}) and Mg^{2+} (46 mmol L^{-1}).

4. Discussion

4.1. Formation of Cd-bearing colloidal particles by dissolution–precipitation

Dissolution-precipitation occurred for DCPD powder that had been soaked in a 500 mg L^{-1} Cd^{2+} solution. The particle size distributions and kinetic light extinction indicated the dissolution of DCPD particles and, in turn, the generation of a new phase in the Cd-rich solution (Fig. 1). As in a previous study (Zhai et al., 2018), the newly generated particles were identified as compounds consisting of cadmium and phosphate (Fig. 2A and E). This transformation to PCDTP may have occurred primarily as a result of heterogeneous nucleation. Rather, the large DCPD particles act as a solid substrate, and etch pits formed on their surface by dissolution also provide surfaces for heterogeneous nucleation. As larger DCPD particles dissolve into various species in a Cd-rich environment as described in Eqs (1)–(3), the solution in the localized space surrounding the particles becomes highly concentrated with the resulting ionic species, whose concentrations exceed the saturation points for cadmium phosphates. According to Eq. (4), because heterogeneous nucleation occurs at lower supersaturation than homogeneous nucleation, dissolved species have a high probability of precipitating on the surface as a new phase with low solubility. The solubilities of DCPD and PCDTP are $K_{sp} = 10^{-6.60}$ and $K_{sp} = 10^{-30.9}$, respectively (Ayati and Madsen, 2001; Gregory et al., 1970). This precipitation route produces new particles that resemble the parent DCPD particles in shape.

The degree of supersaturation within the boundary layer at the particle surface may exceed the requirements for homogeneous nucleation. This allowed the formation of free-standing nuclei and their subsequent growth, followed by collision and coalescence to generate secondary particles (Fig. 2B and F). During the experiments, a transparent Cd solution became cloudy upon adding DCPD powder, indicating that small particles were generated by dissolution–precipitation. However, homogeneous nucleation should be arrested, as precipitation occurring simultaneously on the particle surface rapidly consumes the dissolved species. As a result, some of the particles appeared plate-like, and other aggregates of spheroidal particles were observed. Consequently, the overall dissolution–precipitation process resulted in a decrease in the total volume of the larger particles and an increase in the smaller ones (2.41 times that of DCPD soaked in DIW), resulting in a bimodal size distribution (Fig. 1B).

$$CaHPO_4{\cdot}2H_2O_{(s)} + H_2O_{(l)} \rightarrow Ca^{2+}_{(aq)} + HPO^{2-}_{4(aq)} + 3H_2O_{(l)} \quad (1)$$

$$HPO^{2-}_{4(aq)} + H_2O_{(l)} \rightleftharpoons H_2PO^{-}_{4(aq)} + OH^{-}_{(aq)} \quad (2)$$

$$HPO^{2-}_{4(aq)} + H_2O_{(l)} \rightleftharpoons PO^{3-}_{4(aq)} + H_3O^{+}_{(aq)} \quad (3)$$

$$H_2PO^{-}_{4(aq)} + 3PO^{3-}_{4(aq)} + xCa^{2+}_{(aq)} + (5-x)Cd^{2+}_{(aq)} + 4H_2O_{(l)} \rightarrow Cd_{(5-x)}Ca_xH_2(PO_4)_4{\cdot}4H_2O_{(s)} \quad (4)$$

In summary, the use of inappropriate adsorbents such as DCPD in a water system that gives rise to a high concentration of Cd^{2+} causes serious colloidal-facilitated contamination.

4.2. Heterogeneous nucleation and crystal growth on PANF

Given the harmful effects of the dissolution–precipitation of DCPD powder in the presence of Cd^{2+} in water systems, a new methodology for adsorptive removal using DCPD should be developed. As postulated, the introduction of additional solid surfaces composed of PAN fibers

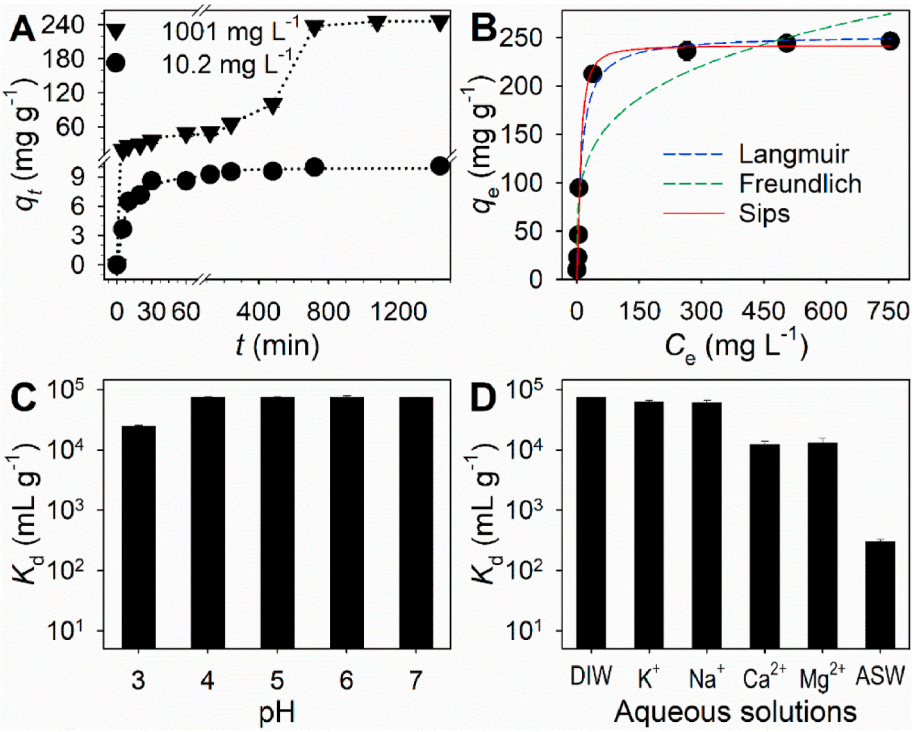

Fig. 4. Cd removal capability of DCPD(100)/PANF: (A) Uptake kinetics at $C_0 = 10.2$ and 1001 mg L^{-1}; (B) Equilibrium adsorption (q_e vs. C_e) at $C_0 = 10$–1000 mg L^{-1} with fittings of Langmuir, Freundlich, and Sips models; Distribution coefficients (K_d) for Cd^{2+} adsorption at $C_0 \cong 10.0$ mg L^{-1}: (C) at varying pH conditions and (D) in the presence of various competing cations at a concentration of 10 mmol L^{-1} and in ASW.

prevented the formation of small colloidal particles containing cadmium. The particle size distributions and kinetic light extinction clearly demonstrated that the PANFs inhibited the formation of suspended particles in the Cd-rich solution (Fig. 1). Similar inhibitory effects were observed in the presence of PANFs with various DCPD loadings (Fig. S2B). As shown in the SEM image of the DCPD(100)/PANF soaked in the 500 mg L^{-1} Cd^{2+} solution (Fig. 2D), some particles appeared at the top of the fibers. Although PAN is highly hydrophilic, the new particles may not form chemical bonds with the PAN fibers. According to a previous study, PANFs exhibited an uptake capacity of 5.89 mg g^{-1} for Sr^{2+} (Vivas et al., 2020), most likely via physical adsorption due to van der Waals interactions or hydrogen bonding. PAN is chemically stable and insoluble in water; therefore, it is difficult for it to form new chemical compounds or complexes. Additionally, the high curvature of PANFs, with an average fiber diameter of <500 nm, impedes the wetting of a new phase over a wide area (Vivas et al., 2020), which is different from a flat surface. At the beginning of the dissolution–precipitation process, nuclei might be formed in a boundary layer at the fiber surfaces by heterogeneous nucleation and then continue to grow into larger particles. Once the nuclei grow to a certain size, the particles can act as support solid substrates for further growth. This is because, as Eq. (5) shows, the energy barrier for nucleation or growth is zero if the substrate and monomers are the same material (Manuel García-Ruiz, 2003; Sear, 2007).

$$\Delta G_{het} = \Delta G_{homo}\left(\frac{1}{2} - \frac{3}{4}\cos\alpha + \frac{1}{4}\cos^3\alpha\right) \quad (5)$$

where ΔG_{het} and ΔG_{homo} are the Gibbs energy barriers for the activation of heterogeneous and homogeneous nucleation, respectively, and α is the contact angle that the nucleus forms with the substrate and α becomes zero for the same material. As a result, the microparticles of the hexagonal columnar morphology could be produced as a surface precipitate (Fig. 2D). These particles mainly consisted of the cadmium phosphate (53.4 wt% Cd and 0.53 wt% Ca, Fig. 2H), *i.e.*, PCDTP. The hexagonal columnar particles did not appear to experience collision or coalescence.

In the other place of the DCPD(100)/PANF sample (Fig. 2C), lumpy particles also existed, which contained more calcium phosphate (30.8 wt % Ca and 14.0 wt% Cd, Fig. 2G) than the columnar particles. The formation route of these lumps may differ from that of the hexagonal columnar particles. As shown in Fig. S3A, during the infusion process in the preparation of DCPD/PANF, a large portion of the DCPD powder appeared to be buried under the layers of PAN fibers. When immersed in the Cd solution, the buried portion did not readily dissolve. This partial exposure may limit the dissolution–precipitation process. As a result, the particle shape did not appear to change and the Cd content was very low. The compounding of a sparingly soluble adsorbent material with PANF prevented the generation of hazardous colloidal particles during the adsorptive removal of toxic metal ions.

ICP-OES analysis of the filtrate for the Cd^{2+} soaking experiments at 500 mg L^{-1} using DCPD and DCPD(100)/PANF showed Cd adsorption of 83.5% and 47.3%, respectively. The amount of Cd adsorbed for the composite was 56.7% of that for DCPD, which is similar to the expectation (50%) from the mass loading in the composite. And the mole ratio between the dissolved Ca and adsorbed Cd were found 1.17 and 1.05 for DCPD and the composite, respectively, indicating that the main adsorption mechanism is dissolution–precipitation or ion exchange between Ca and Cd.

4.3. Cd removal mechanism of DCPD and DCPD/PANF

The Cd removal mechanisms of DCPD and DCPD/PANF involved ion exchange, complexation, dissolution, crystal transformation, nucleation, and growth (Fig. 5). These complex behaviors appeared to differ depending on the concentration of Cd and the availability of a solid surface around the DCPD particles. In this study, dissolution–precipitation behavior was investigated at pH ≅ 7.0 because pH, *i.e.*, proton concentration, greatly influences the dissolution characteristics of DCPD. This pH condition may limit the degree of

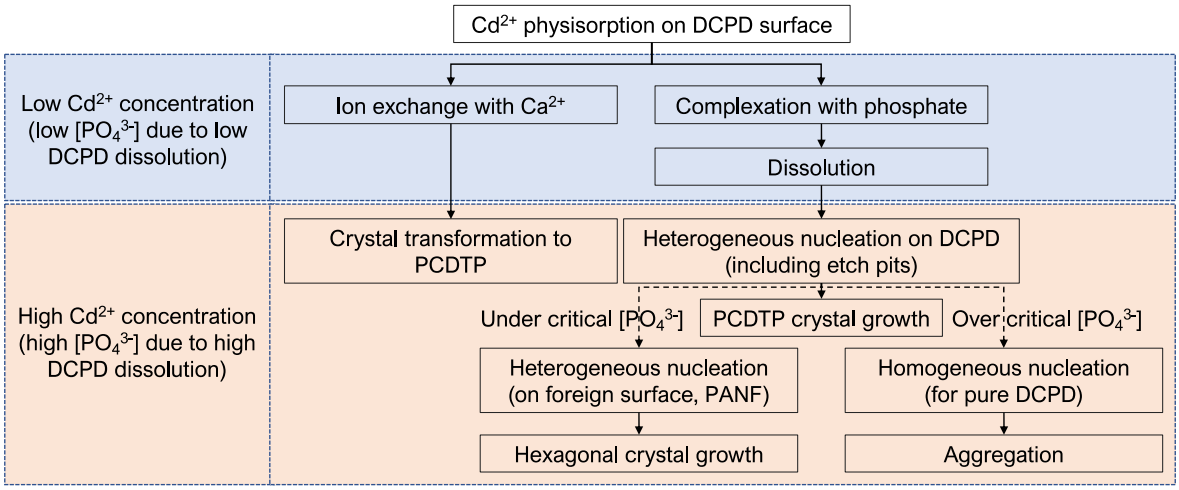

Fig. 5. Schematic for adsorption of Cd^{2+} and concurrent crystal formation on DCPD and DCPD/PANF via dissolution–precipitation.

dissolution, thereby enabling us to focus on the DCPD-water interface with a low-to-moderate degree of supersaturation of the dissolved species.

At a low Cd concentration of 10 mg L^{-1}, Cd^{2+} ions are physically adsorbed on the DCPD surface or form complexes with the oxygen atoms of phosphate sites ($\equiv PO^{-}$) that are deprotonated (the pzc of DCPD is pH ~6.2). In addition, Cd^{2+} ions may directly replace Ca ions in the Ca-terminated polar sites on the DCPD surface (Qin et al., 2013). As the amount of adsorbed Cd increases, Cd^{2+} ions tend to replace Ca^{2+} ions in the DCPD structure via solid-state diffusion. Because of the relatively low Cd concentration, ion exchange was confined within the near-surface interlayers, and structural transformation may not have occurred (Fig. 3F). The dissolution of DCPD appeared to be negligible into altering the behavior of the Cd and phosphate species around the interface, thereby eliminating the apparent precipitation of the new Cd–P phase.

At a high Cd concentration of 500 mg L^{-1}, the Cd^{2+} ions in the aqueous solution replaced the Ca^{2+} ions, similar to the low Cd concentration case. Because of the high Cd concentration gradient at the DCPD-water interface, the adsorbed Cd^{2+} ions moved further toward the inner sites of the DCPD structure, resulting in a crystal transformation to PCDTP. Although solid-state diffusion across grain boundaries or lattice vacancies is slow, it can cause the crystal structure to transform into cadmium phosphates such as amorphous phase and crystalline $Cd_5H_2(PO_4)_4{\cdot}4H_2O$ and $Cd_5(PO_4)_3OH$. In DCPD, Cd^{2+} ions were known to be accommodated in lattice vacancies and substituted with Ca^{2+} ions in the structure (Zhai et al., 2018). Besides, the complexation of Cd ions with surface phosphates leads to apparent dissolution at the (010) face of DCPD, releasing Ca^{2+} and HPO_4^{2-} ions into the boundary layer of the DCPD-water interface (Qin et al., 2013; Zhai et al., 2018). Cd^{2+} and NO_3^{-} may alter the hydration layer near the (010) face, dislodging water molecules from Ca^{2+} and HPO_4^{2-} ions, thereby promoting their dissolution (Kowacz and Putnis, 2008). Consequently, higher concentrations of Ca^{2+} and HPO_4^{2-} in the boundary layer lead to the nucleation of the Cd–P phases (Zhai et al., 2018). Inside the film of the interfacial boundary layer of fluid, dissolved species could be supersaturated with respect to the solid phases that have a low solubility. At critical supersaturation, heterogeneous nucleation first occurred on the parent DCPD surface because its energy barrier was lower than that of homogeneous nucleation. All the surfaces exposed to the water interface, including the etch pits formed by dissolution, participated in this precipitation. The nuclei formed on the DCPD surface continued to grow as the dissolved species dissipated. Because the solubility of PCDTP is much lower than that of DCPD, PCDTP forms a new phase, with a lower molar volume than DCPD. The significant difference in the relevant molar volume between DCPD and PCDTP (65.2%) causes the resulting structure to become porous (Pollok et al., 2011). The much less volume occupied by a new cadmium phase implies that the crystallographic structural matching is lower (Prieto et al., 2003). This porosity allows the fluid phase to infiltrate further toward the DCPD surface intact, thus allowing the dissolution–precipitation to continue. Hence, the PCDTP structure was formed on top of the native DCPD (Fig. 2A and C). However, a high concentration of Ca^{2+} in the boundary film may inhibit the complete dissolution of DCPD.

At the outset of dissolution at a high Cd concentration, the dissolved species in the fluid inside the film layer could reach a point above the critical supersaturation that allows homogeneous nucleation. Newly formed nuclei in the thin film may undergo collision and coalescence to form secondary aggregates. Because the slow dissolution of DCPD at pH $\leqq$ 7.0 should allow limited supersaturation, the formation of aggregates from homogeneous nucleation is finite. Moreover, as dissolution–precipitation proceeds, the adsorbent surface becomes porous, leaving less area exposed to the fluid phase. Nevertheless, this period of homogeneous nucleation and growth cannot be completely avoided (Fig. 2B).

In contrast, the local high supersaturation in the narrow region around the DCPD-water interface could be relieved by introducing more solid surfaces on which heterogeneous nucleation depletes the dissolved species. Thus, the presence of foreign surfaces, such as PANFs, prevents homogeneous nucleation. Once the nuclei were generated on the PANF surface, they continued to grow faster than on the DCPD surface. The Gibbs energy barrier for nucleation or condensation on a solid surface with the same structure is minimal (Eq. (5)). Consequently, heterogeneous nucleation on the foreign PANF surface led to a well-defined crystalline phase of PCDTP (Figs. 2D and 3I). Therefore, the PANF can prevent the generation of small aggregates of Cd-bearing particles.

4.4. *Effectiveness of DCPD(100)/PANF for adsorptive Cd^{2+} removal*

As the main purpose of the design of a composite adsorbent is to achieve high pollutant-removal performance, we conducted a series of typical batch adsorption experiments. Kinetically, Cd^{2+} adsorption on DCPD(100)/PANF at C_0 = 10 mg L^{-1} reached equilibrium after 12 h (Fig. 4A), which ranked low among the existing Cd adsorbents (Table S2). However, the composite could remove 90.9% of Cd^{2+} from water in the first 2 h. At a high concentration of C_0 = 1000 mg L^{-1}, multistage Cd^{2+} uptake kinetics was observed, which is similar to the multistep adsorption kinetics in cobalt removal using DCPD powders (Vivas and Cho, 2021). The second steep adsorption after the first plateau may correspond to dissolution–precipitation. A certain

induction time was required for the precipitation to occur in the interfacial layer at a critical supersaturation by building up ions (Zhai et al., 2018). The Cd adsorption capacity of DCPD(100)/PANF was estimated at 246 mg g^{-1}, which is ranked intermediate among the existing Cd adsorbents (Table S2). This capacity mostly relies on the substitution of the structural Ca^{2+} of DCPD with Cd^{2+} and is lower than that of several Cd adsorbents with more exchangeable interlayer cations or cation-binding surface functional groups.

With regard to the distribution coefficient K_d, DCPD(100)/PANF exhibited an intermediate value at C_0 = 10 mg L^{-1} and pH ≅ 7.0 compared to the existing adsorbents (Table S2). The significant inhibitory effect of divalent cations on Cd^{2+} adsorption on the composite fibers compared to that of monovalent cations can be explained in two ways. Chemical affinity plays a key role in adsorption, which is accompanied by ion exchange. Lewis soft base PO_4^{3-} at the DCPD surface has higher affinity for the relatively soft acids Cd^{2+} (chemical hardness η = 10.29 eV) than for the hard acids Na^+ (η = 21.07 eV), K^+ (η = 13.64 eV), Mg^{2+} (η = 32.55 eV), and Ca^{2+} (η = 19.52 eV) (Lide, 2005; Pearson, 1988). The electrostatic interaction between divalent cations and basic oxygens in phosphates at the surface may be greater than that for monovalent cations. At high ionic strengths, positive ions are surrounded by a high density of negative ions; thus, their electric field is screened or compressed. The compressed electric double layer weakened the electrostatic interactions between the cations and phosphates. The ionic strengths of the $Mg(NO_3)_2$ and $Ca(NO_3)_2$ solutions were three times those of the $NaNO_3$ and KNO_3 solutions at the same cationic concentration. Nevertheless, the radius of the hydrated ion (r_{hyd}), the interatomic distance between the ion and the oxygen atom of a water molecule in the hydration shell, becomes smaller as cationic charge increases (Ichieda et al., 2003). The r_{hyd} of Mg^{2+} (0.209 nm), Ca^{2+} (0.240 nm), and Cd^{2+} (0.230 nm) are smaller than that of Na^+ (0.244 nm) and K^+ (0.281 nm) (Ichieda et al., 2003). Assuming a stronger electrostatic interaction for divalent cations, which is proportional to the charge and inversely proportional to the ionic radius, Mg^{2+} and Ca^{2+} significantly influenced the distribution coefficient for Cd^{2+} of DCPD (100)/PANF. In the ASW, the concentrations of Ca^{2+} (8 mmol L^{-1}) and Mg^{2+} (46 mmol L^{-1}) were two orders of magnitude higher than that of Cd^{2+} (0.089 mmol L^{-1}). In particular, highly concentrated Ca^{2+} ions resist the dissolution of calcium phosphate (*i.e.*, DCPD) according to per Le Chatelier's principle and compete for adsorption sites with Cd^{2+} ions. Thus, DCPD and DCPD(100)/PANF can be regarded as inappropriate for seawater systems containing low Cd concentrations.

5. Conclusions

Sparingly soluble adsorbents used to remove toxic metal ions have been found to produce suspended particles comprising toxic metals via the dissolution–precipitation mechanism in the current and previous studies. In particular, the submicron portion of colloidal particles causes the unapparent problem of microscopic toxic metal transport because they are highly mobile in water. This colloid-facilitated contamination should not be ignored because it is an important pathway for strongly adsorbable contaminants. To prevent colloidal particle formation, we introduced PAN fibers as a supporting substrate for the heterogeneous nucleation of the Cd precipitate and particle growth, which results from the dissolution–precipitation of DCPD in an aqueous Cd^{2+} solution. Consequently, the PANF-supported DCPD did not form free Cd-bearing particles, implying high-to-permanent immobilization of Cd^{2+}. The findings in this work provide an essential understanding on how a solid support assists a sparingly soluble adsorbent in suppressing the formation of mobile hazardous pollutant-bearing colloids. Sparingly soluble compounds such as phosphates, carbonates, hydroxides, sulfates, and oxides may be compounded with PANF to prevent toxic colloid generation. Compounding with PANF should be an effective means, as the application of DCPD powder requires a carrier or support, such as a membrane filter or small beads, to reliably manipulate it.

Credit author statement

Eleazer L. Vivas: Investigation, Visualization, Writing – original draft. Keon-Woo Kim: Investigation. Yong Jae Suh: Conceptualization, Validation, Writing – review & editing. Kuk Cho: Conceptualization, Validation, Writing – review & editing, Supervision.

Associated content

The Supporting Information is available free of charge.

Declaration of competing interest

The authors declare the following financial interests/personal relationships which may be considered as potential competing interests: Kuk Cho reports financial support was provided by National Research Foundation of Korea. Yong Jae Suh reports financial support was provided by Korea Ministry of Science and ICT.

Data availability

Data will be made available on request.

Acknowledgments

This work was supported by the Basic Science Research Program through the National Research Foundation (NRF) of Korea funded by the Ministry of Education, Republic of Korea (2020R1A6A1A03044834; 2022R1I1A3063150) and by the Basic Research Project (GP 2022-011, 23–3212-2) of the Korea Institute of Geoscience and Mineral Resources (KIGAM) funded by the Ministry of Science and ICT of Korea.

Appendix A. Supplementary data

Supplementary data to this article can be found online at https://doi.org/10.1016/j.jenvman.2023.118345.

References

Astilleros, J.M., Pinto, A.J., Goncalves, M.A., Sanchez-Pastor, N., Fernandez-Diaz, L., 2013. In situ nanoscale observations of metatorbernite surfaces interacted with aqueous solutions. Environ. Sci. Technol. 47, 2636–2644. https://doi.org/10.1021/es302781k.

Ayati, M., Madsen, H.E.L., 2001. Solubility product of the cadmium phosphate $Cd_5H_2(PO_4)_4{\cdot}4H_2O$ at 37 °C. J. Chem. Eng. Data 46, 113–116. https://doi.org/10.1021/je000199v.

Cao, X., Ma, L.Q., Rhue, D.R., Appel, C.S., 2004. Mechanisms of lead, copper, and zinc retention by phosphate rock. Environ. Pollut. 131, 435–444. https://doi.org/10.1016/j.envpol.2004.03.003.

Googerdchian, F., Moheb, A., Emadi, R., 2012. Lead sorption properties of nanohydroxyapatite-alginate composite adsorbents. Chem. Eng. J. 200, 471–479. https://doi.org/10.1016/j.cej.2012.06.084.

Gregory, T.M., Moreno, E.C., Brown, W.E., 1970. Solubility of $CaHPO_4 \cdot 2H_2O$ in the system $Ca(OH)_2$-H_3PO_4-H_2O at 5, 15, 25, and 37.5 °C. J Res Natl Bur Stand A Phys Chem 74a, 461–475. https://doi.org/10.6028/jres.074A.036.

Guren, M.G., Putnis, C.V., Montes-Hernandez, G., King, H.E., Renard, F., 2020. Direct imaging of coupled dissolution-precipitation and growth processes on calcite exposed to chromium-rich fluids. Chem. Geol. 552, 119770 https://doi.org/10.1016/j.chemgeo.2020.119770.

Ichieda, N., Kasuno, M., Banu, K., Kihara, S., Nakamatsu, H., 2003. Evaluation of hydration enthalpies of monatomic cations by considering both long-range and short-range interactions. J. Phys. Chem. 107, 7597–7603. https://doi.org/10.1021/jp0348171.

Jang, S.H., Min, B.G., Jeong, Y.G., Lyoo, W.S., Lee, S.C., 2008. Removal of lead ions in aqueous solution by hydroxyapatite/polyurethane composite foams. J. Hazard Mater. 152, 1285–1292. https://doi.org/10.1016/j.jhazmat.2007.08.003.

Joseph, C., Balboni, E., Baumer, T., Treinen, K., Kersting, A.B., Zavarin, M., 2019. Plutonium desorption from nuclear melt glass-derived colloids and implications for migration at the Nevada national security site, USA. Environ. Sci. Technol. 53, 12238–12246. https://doi.org/10.1021/acs.est.9b03956.

Kowacz, M., Putnis, A., 2008. The effect of specific background electrolytes on water structure and solute hydration: consequences for crystal dissolution and growth. Geochem. Cosmochim. Acta 72, 4476–4487. https://doi.org/10.1016/j.gca.2008.07.005.

Le, Q.T.N., Vivas, E.L., Cho, K., 2021. Calcium oxalate/calcium silicate hydrate (Ca-Ox/C-S-H) from blast furnace slag for the highly efficient removal of Pb^{2+} and Cd^{2+} from water. J. Environ. Chem. Eng. 9, 106287 https://doi.org/10.1016/j.jece.2021.106287.

Li, J., Bai, R., Chen, W., Ren, C., Yang, F., Tian, X., Xiao, X., Zhao, F., 2023. Efficient lead immobilization by bio-beads containing Pseudomonas rhodesiae and bone char. J. Hazard Mater. 447, 130772 https://doi.org/10.1016/j.jhazmat.2023.130772.

Lide, D.R., 2005. CRC Handbook of Chemistry and Physics, 85th ed. CRC Press, Boca Raton.

Manuel García-Ruiz, J., 2003. Nucleation of protein crystals. J. Struct. Biol. 142, 22–31. https://doi.org/10.1016/S1047-8477(03)00035-2.

Mashal, K., Harsh, J.B., Flury, M., Felmy, A.R., Zhao, H.T., 2004. Colloid formation in Hanford sediments reacted with simulated tank \waste. Environ. Sci. Technol. 38, 5750–5756. https://doi.org/10.1021/es0349709.

McDowell, H., Gregory, T.M., Brown, W.E., 1977. Solubility of $Ca_5(PO_4)_3OH$ in the system $Ca(OH)_2$-H_3PO_4-H_2O at 5, 15, 25, and 37.5 °C. J Res Natl Bur Stand A Phys Chem 81a, 273–281. https://doi.org/10.6028/jres.081A.017.

Medellín-Castillo, N.A., Cruz-Briano, S.A., Leyva-Ramos, R., Moreno-Piraján, J.C., Torres-Dosal, A., Giraldo-Gutiérrez, L., Labrada-Delgado, G.J., Pérez, R.O., Rodriguez-Estupiñan, J.P., Reyes Lopez, S.Y., Berber Mendoza, M.S., 2020. Use of bone char prepared from an invasive species, pleco fish (Pterygoplichthys spp.), to remove fluoride and Cadmium(II) in water. J. Environ. Manag. 256, 109956 https://doi.org/10.1016/j.jenvman.2019.109956.

Morales, J., Astilleros, J.M., Fernandez-Diaz, L., Alvarez-Lloret, P., Jimenez, A., 2013. Anglesite ($PbSO_4$) epitactic overgrowths and substrate-induced twinning on anhydrite ($CaSO_4$) cleavage surfaces. J. Cryst. Growth 380, 130–137. https://doi.org/10.1016/j.jcrysgro.2013.06.010.

Pearson, R.G., 1988. Absolute electronegativity and hardness: application to inorganic chemistry. Inorg. Chem. 27, 734–740. https://doi.org/10.1021/ic00277a030.

Plathe, K.L., von der Kammer, F., Hassellov, M., Moore, J.N., Murayama, M., Hofmann, T., Hochella, M.F., 2013. The role of nanominerals and mineral nanoparticles in the transport of toxic trace metals: field-flow fractionation and analytical TEM analyses after nanoparticle isolation and density separation. Geochem. Cosmochim. Acta 102, 213–225. https://doi.org/10.1016/j.gca.2012.10.029.

Pollok, K., Putnis, C.V., Putnis, A., 2011. Mineral replacement reactions in solid solution-aqueous solution systems: volume changes, reactions paths and end-points using the example of model salt systems. Am. J. Sci. 311, 211–236.

Prieto, M., Cubillas, P., Fernández-Gonzalez, Á., 2003. Uptake of dissolved Cd by biogenic and abiogenic aragonite: a comparison with sorption onto calcite. Geochem. Cosmochim. Acta 67, 3859–3869. https://doi.org/10.1016/S0016-7037(03)00309-0.

Qin, L., Zhang, W., Lu, J., Stack, A.G., Wang, L., 2013. Direct imaging of nanoscale dissolution of dicalcium phosphate dihydrate by an organic ligand: concentration matters. Environ. Sci. Technol. 47, 13365–13374. https://doi.org/10.1021/es402748t.

Renard, F., Putnis, C.V., Montes-Hernandez, G., King, H.E., Breedveld, G.D., Okkenhaug, G., 2018. Sequestration of antimony on calcite observed by time-resolved nanoscale imaging. Environ. Sci. Technol. 52, 107–113. https://doi.org/10.1021/acs.est.7b04727.

Ryan, J.N., Elimelech, M., 1996. Colloid mobilization and transport in groundwater. Colloids Surf. A Physicochem. Eng. Asp. 107, 1–56. https://doi.org/10.1016/0927-7757(95)03384-X.

Sear, R.P., 2007. Nucleation: theory and applications to protein solutions and colloidal suspensions. J. Phys. Condens. Matter 19, 033101. https://doi.org/10.1088/0953-8984/19/3/033101.

Tang, X.Y., Weisbrod, N., 2009. Colloid-facilitated transport of lead in natural discrete fractures. Environ. Pollut. 157, 2266–2274. https://doi.org/10.1016/j.envpol.2009.03.034.

Vivas, E.L., Cho, K., 2021. Efficient adsorptive removal of Cobalt(II) ions from water by dicalcium phosphate dihydrate. J. Environ. Manag. 283.

Vivas, E.L., Lee, S., Cho, K., 2020. Brushite-infused polyacrylonitrile nanofiber adsorbent for strontium removal from water. J. Environ. Manag. 270, 110837 https://doi.org/10.1016/j.jenvman.2020.110837.

Wang, L.J., Putnis, C.V., King, H.E., Hovelmann, J., Ruiz-Agudo, E., Putnis, A., 2017. Imaging organophosphate and pyrophosphate sequestration on brucite by in situ atomic force microscopy. Environ. Sci. Technol. 51, 328–336. https://doi.org/10.1021/acs.est.6b05456.

Wang, L.J., Putnis, C.V., Ruiz-Agudo, E., Hovelmann, J., Putnis, A., 2015. In situ imaging of interfacial precipitation of phosphate on goethite. Environ. Sci. Technol. 49, 4184–4192. https://doi.org/10.1021/acs.est.5b00312.

Wang, P.L., Shen, T.T., Li, X.Y., Tang, Y.Y., Li, Y.J., 2020. Magnetic mesoporous calcium carbonate-based nanocomposites for the removal of toxic Pb(II) and Cd(II) ions from water. ACS Appl. Nano Mater. 3, 1272–1281. https://doi.org/10.1021/acsanm.9b02036.

Wei, Y.Q., Yuan, C.P., Xu, X.Y., Chen, X., Ren, Z.F., Gui, X.Y., Zhao, L., Qiu, H., Cao, X.D., 2022. Colloid formation and facilitated chromium transport in the coastal area soil induced by freshwater and seawater alternating fluctuations. Water Res. 218, 118456 https://doi.org/10.1016/j.watres.2022.118456.

Wolfsberg, A., Dai, Z.X., Zhu, L., Reimus, P., Xiao, T., Ware, D., 2017. Colloid-facilitated plutonium transport in fractured tuffaceous rock. Environ. Sci. Technol. 51, 5582–5590. https://doi.org/10.1021/acs.est.7b00968.

Yamashita, M., Wannagon, A., Matsumoto, S., Akai, T., Sugita, H., Imoto, Y., Komai, T., Sakanakura, H., 2010. Leaching behavior of CRT funnel glass. J. Hazard Mater. 184, 58–64. https://doi.org/10.1016/j.jhazmat.2010.08.002.

Zhai, H., Wang, L., Qin, L., Zhang, W., Putnis, C.V., Putnis, A., 2018. Direct observation of simultaneous immobilization of cadmium and arsenate at the brushite–fluid interface. Environ. Sci. Technol. 52, 3493–3502. https://doi.org/10.1021/acs.est.7b06479.

Zhou, C.L., Song, X., Wang, Y.W., Wang, H., Ge, S.F., 2022. The sorption and short-term immobilization of lead and cadmium by nano-hydroxyapatite/biochar in aqueous solution and soil. Chemosphere 286, 131810. https://doi.org/10.1016/j.chemosphere.2021.131810.